Supplementary Material for

Non-Canonical Protein Kinase A Activation by Oligomerization of Regulatory Subunits as Revealed by Inherited Carney Complex Mutations

Naeimeh Jafari[1], Jason Del Rio[2], Madoka Akimoto[1], Jung Ah Byun[3], Stephen Boulton[3], Kody Moleschi[1], Yousif Al Sayyed[1], Pascale Swanson[3], Jinfeng Huang[1], Karla Martinez Pomier[1], Chi Lee, Jian Wu[2], Susan S. Taylor[2,4], Giuseppe Melacini[1,3*]

[1]Department of Chemistry and Chemical Biology, McMaster University, 1280 Main St. W. Hamilton, Canada; [2]Department Pharmacology, University of California San Diego, La Jolla, CA 92093-0653, USA; [3]Department of Biochemistry and Biomedical Sciences, McMaster University, 1280 Main St. W. Hamilton, Canada; [4]Departments of Chemistry and Biochemistry, University of California San Diego, La Jolla, CA 92093-0653, USA

Running title: *PKA C Activation by PKA R Oligomerization*

*To whom correspondence may be addressed. Email: staylor@ucsd.edu or melacin@mcmaster.ca

This supplementary Materials includes:

Materials and Methods

Protein Purification. Mutants were prepared by site-directed mutagenesis. All constructs were transformed in BL21(DE3) cells and expressed in LB broth for unlabeled 1-379 bPKA R1α constructs, and in ^{15}N-M9 media for uniformly ^{15}N-labeled 119-379 and 96-244 bPKA R1α constructs. Expression and purification were implemented based on previously published protocols (1–5). Cells were grown at 37 °C up until the optical density at 600 nm reached 0.6 – 0.7 and then they were induced with 0.5 mM isopropyl-1-thio-β-D-galactopyranoside for 17 hours at 18 °C. Cells were then resuspended in 20 mM MES buffer, pH 6.5 and 100 mM NaCl (buffer A) and disrupted with a protein homogenizer operating at 20 psi. The cell debris was removed through centrifugation (one hour at 14,000 rpm). After gradual fractionation with 40 % ammonium sulfate, the protein was resuspended in buffer A with 2 mM EGTA, 2 mM EDTA, and 5 mM DTT (buffer B) and incubated with a cAMP-Sepharose resin overnight at 4 °C. The resin-bound protein was washed with buffer B, buffer B with 700 mM NaCl, and buffer B at room temperature. Then PKA R1α was eluted by using 25 – 40 mM cAMP or 20 mM cGMP depending of the purpose of the experiment. The cGMP eluted protein was dialysed extensively against 50 mM MOPS buffer pH 7.0, 100 mM NaCl, 0.5 mM EDTA, 5 mM DTT (buffer C) prior to gel filtration. Further purification was obtained through gel filtration on a HiLoad 16/600 Superdex 200 pg column, which had been pre-equilibrated with buffer C for the 1-379 construct and with 50 mM MES buffer, pH 6.5, 100 mM NaCl, 2 mM EGTA, 2 mM EDTA, and 5 mM DTT (buffer D) for the 119-379 constructs. Purification of the 96-244 PKA R1α fusion construct with a His_6-small ubiquitin-related modifier (SUMO) tag was based on nickel-NTA (nitrilotriacetic acid) affinity chromatography with 50 mM MOPS buffer pH 7.0 and 100 mM NaCl. After cleavage of the His_6-SUMO tag with a His_6-tagged tobacco etch virus (TEV) protease, a second nickel-NTA column was utilized to remove the cleaved His_6-SUMO and TEV. The apo 96-244 construct was prepared by unfolding with 8 M urea and refolding by gradual decrease of urea concentration when protein was bound to the first nickel column. Further purification of the 96-244 construct was implemented through gel filtration on a Superdex 75 column pre equilibrated with 50 mM MOPS buffer pH 7.0, 100 mM NaCl, and 10 mM $MgCl_2$. Protein concentrations were measured through the Bradford assay using bovine serum albumin as standard protein.

Urea Unfolding. The assay was implemented in buffer C (50 mM MOPS buffer pH 7.0, 100 mM NaCl, 0.5 mM EDTA, 5 mM DTT) with 5 μM of the PKA R1α 1-379 or 96-244 construct and with or without 100-fold excess of cAMP. The protein samples were incubated for three hours at room temperature with urea concentrations increasing from 0 to 8 M. Upon excitation at 293 nm, tryptophan emission was checked at 305-450 nm using a BioTek Cytation5 microplate reader. Unfolding was tracked by the ratio of fluorescence intensity at 353 nm / 340 nm and the fraction of unfolded protein as $X_U=(R-R_N)/(R_U-R_N)$, where R is the observed intensity's ratio at each urea concentration, and R_N is the R value of the folded protein in the absence of urea, and R_U is the R value at 8 M urea concentration. The unfolding assays were performed in triplicate. Errors were estimated based on standard deviations between triplicates or at plateau.

NMR Experiments. All NMR experiments were implemented on Bruker AV700 spectrometer. 1D ^{1}H NMR spectra for 8 μM R1α (1-379) were acquired at 298K in 20 mM phosphate buffer pH 7.4, 50 mM NaCl, 100 % D_2O in the presence of 80 μM excess cAMP with a spectral width of 16.23 ppm and 16K points. The repetition delay was 1 s. The number of scans was 512. Spectra were

processed with a line broadening of 3.0 Hz. After 90 minutes of incubation at 60 °C (referred to here as mild heat treatment), 1D ^{1}H NMR spectra were reacquired. In Figure 4B, the methyl peak intensity of wt and A211T prior to mild heat treatment were normalized to the methyl intensity of A211D prior to mild heat treatment. The same normalization scaling constant was applied to the intensity of the mildly-heat-treated samples as well. Unless otherwise specified, the ^{1}H,^{15}N-HSQC spectra of 100-200 μM R1α (119-379) were acquired in buffer D (50 mM MES buffer, pH 6.5, 100 mM NaCl, 2 mM EGTA, 2 mM EDTA, and 5 mM DTT) with 10 % D_2O and 0.7-1.2 mM excess cAMP at 306 K using 1024 and 128 complex t_2 and t_1 points, respectively, 8 scans and a 1.0 s recycle delay. The H/D exchange samples were prepared based on previously published protocols and spectra were analysed based on previous assignments (2). The H/D exchange buffer was the same as the HSQC buffer, but was prepared in 99% D_2O and 0.7 mM cAMP. The R1α (119-379) concentrations for the H/D exchange experiments were in the 140-260 μM range. The dead time for H/D exchange experiments was ~25 ± 5 minutes. The presence of excess cAMP and protein was monitored by 1D ^{1}H NMR spectra interleaved between the acquisition of the HSQC spectra for monitoring H/D exchange.

ThT and ANS Fluorescence, DLS, and TEM Data Acquisition. All the fluorescence data were acquired using a BioTek Cytation5 plate reader. For these experiments we prepared 8 μM R1α (1-379) with ten-fold excess cAMP in buffer C with either 50 μM Thioflavin (ThT) or 200 μM 1-Anilino-8-Napthalene Sulfonate (ANS). The ANS fluorescence spectra were first recorded at 298K with excitation at 350 nm and emission range of 400-600 nm. Samples were then heated to 60 °C and the ThT fluorescence was monitored with excitation at 440 nm and emission at 482 nm every five minutes for a total of 14 hours. After 14 hours of incubation at 60 °C (referred to here as heat treatment), the ANS fluorescence spectra were re-acquired and the initial ANS fluorescence spectra subtracted. Triplicates spectra were acquired for each A211 mutant. For the G287 mutants, the error for the ThT fluorescence was assessed as the standard deviation of ten data points recorded at the end of the 13 hours and 20 minutes incubation period at 60 °C, while the error for the ANS fluorescence was computed as the standard error of two replicates. DLS data were acquired using the same sample utilized for the ThT experiments after 1:2 dilution with buffer C. Prior to DLS measurements, samples were centrifuged at 13,000 rpm for ten minutes. A Malvern ZEN3600 – Zetasizer Nano ZS with 1.5 mL cuvettes and a 1 cm pathway was used for DLS data acquisition at 298K. The DLS profiles are the average of three technical replicates. The samples for the TEM images were prepared according to the same protocol used for the ThT experiments followed by 3:16 dilution with ultrapure water. 5 μL aliquots were loaded on carbon coated grids and after two minutes of incubation, the grids were washed with 100 μL ultrapure water and negatively stained with 1 % uranyl acetate for one minute. The TEM images were acquired at 80 kV on a JEOL 1200EX TEMSCAN. Negative control samples for DLS and TEM were not subject to heat treatment, but incubated at 4 °C and contained 8 μM R1α (1−379) wt or mutant proteins with tenfold excess cAMP.

PKA Inhibition Assay. The activation of bovine heart C-subunit PKA (Sigma-Aldrich P2645) was measured through the Kinase-Glo luminescent assay (Promega). After 30-minute incubation at room temperature of 4 nM C-subunit in the presence of 0-60 nM R1α (1-379), we added 10 μM ATP and 5 μM Kemptide. The final volume of the reaction mixture was 50 μL. The reaction was quenched after an hour incubation at room temperature by the addition of 50 μL of Ultra-Glo Luciferase reagent (Promega). After ten minutes at room temperature, the luminescence was

recorded by a BioTek Cytation5 microplate reader. The buffer assay was Tris:HCl 40 mM pH 7.5, BSA 0.1 mg/ml, and $MgCl_2$ 20 mM and three biological replicates were acquired. Errors were estimated based on standard deviations among triplicate measurements. The R1α proteins were prepared by eluting with cGMP as described in the Supplementary Text. Unless otherwise specified, samples with oligomerized R1α were prepared by incubating at 37 °C for 2-8 hours 1 μM of natively folded R1α. Control samples from the same solution of 1 μM natively folded R1α were stored at 4 °C for 2-8 hours. Percentage inhibition was calculated relative to wt R1α kept at 4 °C for two hours. Concentrations after incubation were monitored by a NanoDrop™ One/One^C Microvolume UV-Vis Spectrophotometer.

Protein Crystallization and Data Collection. Purified PKA R1α (1-379) A211D Carney Complex mutant was concentrated in 30 kDa MWCO Amicon filters (Millipore; Burlington, MA) to 8 mg/mL. The protein was crystallized in 2 μL hanging drops using the vapor diffusion method with 75 mM Sodium Acetate (pH 5.0), 2.0 M sodium formate, and four-fold molar excess cAMP at 22.5 °C. Tetragonal crystals formed in approximately two weeks and were transferred to a cryoprotectant solution comprised of the mother liquor supplemented with 40% glycerol prior to flash freezing in liquid nitrogen. Further details about molecular replacement and structure refinement are available in the Supplementary Information.

Molecular Replacement and Structure Refinement. X-ray diffraction data were collected at the Advanced Light Source 822 beamline (Berkley, CA) and scaled in a R3 space group (a=b=176.8 Å, c= 345.5 Å) using HKL2000 (6). Initial phasing of the RIα A211D dimer was generated by molecular replacement, using the monomeric $RI\alpha_{91\text{-}379}$ (PDB ID: 1RGS) as a search model probe in Phaser (7, 8). Phaser models were improved by solvent flattening using Density Modification (DM)(9). Model building was performed in Coot, using the crystallography and NMR systems (CNS) coupled with refmac noncrystallographic symmetry restraints and followed by multiple rounds of refinement using Phenix.(10–13) Implementing TLS refinement for each chain converged to R and R_{free} values of 0.221 and 0.269, respectively (Table S2)(14). The final model was comprised of four individual dimers each containing residues 109–376, and verified with PROCHECK for excellent geometry(15). In contrast to wild type, which crystallized as a single dimer in a tetragonal $P4_12_12$ space group, the A211D mutant packed in a trigonal R3 space group comprised of four individual dimers (I-IV; Table S2; Figure S5A). All figures, SASA and RMSD values were prepared or calculated using PyMOL Molecular Graphics System, Version 2.4.0 (Schrödinger, LLC; San Diego, CA) or PISA (16).

Trypsin digestion. Full length WT PKA R1α (no excess cAMP) and A211D mutant (no excess cAMP) at 15 μg/50 μL were incubated with trypsin 0.0125 % for 1h at 37 °C. Buffer C (50 mM MOPS buffer pH 7.0, 100 mM NaCl, 0.5 mM EDTA, 5 mM DTT) was used to dilute the samples. After centrifugation, the samples were analyzed with SDS-page and CBB stain.

Figure S1

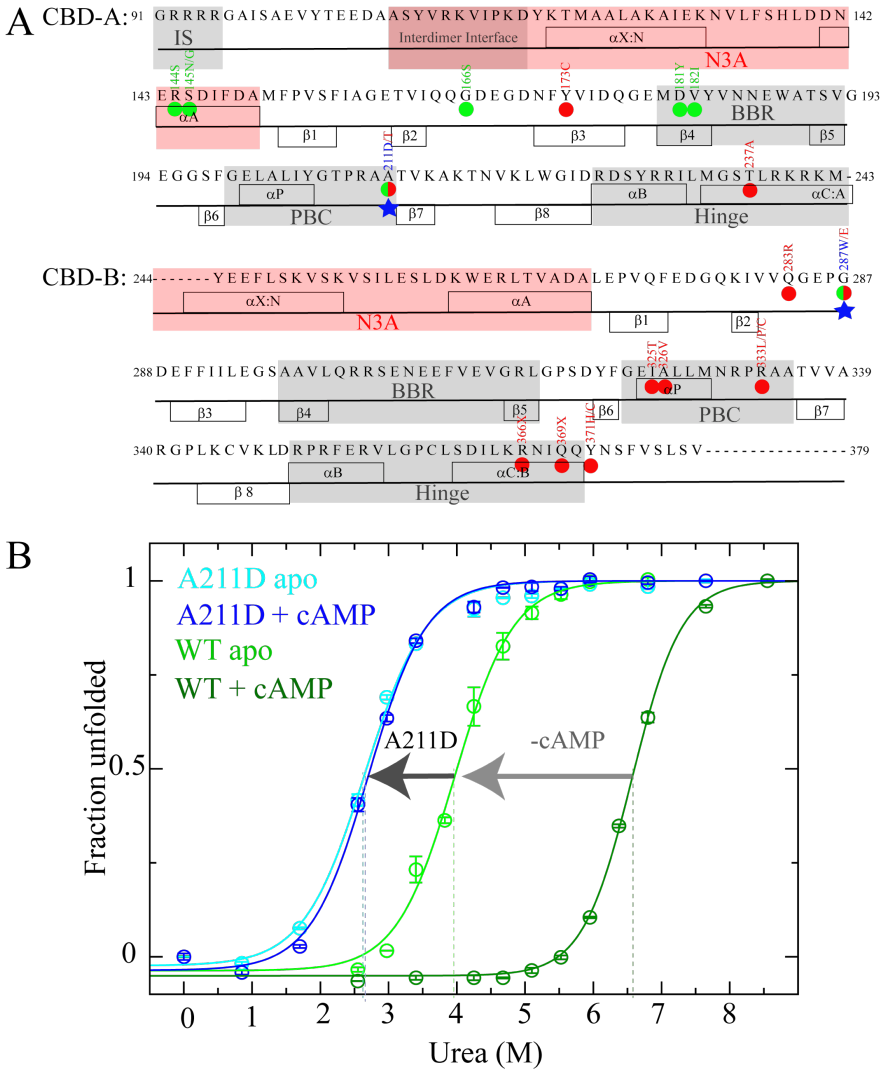

Figure S1: (A) Sequence and secondary structure of the tandem cAMP-binding domains (CBDs). Red/gray areas are binding or allosteric hot spots. IS is the inhibitory site, PBC the phosphate binding cassette, BBR the base binding region. The blue stars denote the double CNC/ACRDYS1 mutant sites Ala 211 and Gly 287. Other non haplo-insufficient CNC and ACRO mutants are indicated in green and red, respectively. (B) *Effect of the A211D Mutation on the Stability of PKA R1α CBD-A.* Urea unfolding profiles of 5 µM wt and A211D PKA R1α (96-244) spanning CBD-A in the absence and presence of 100-fold excess cAMP. The color code is shown in the figure. The vertical dashed lines indicate the urea concentrations needed for half-maximal unfolding (C_m). Data acquired in triplicate and error is SD.

Figure S2

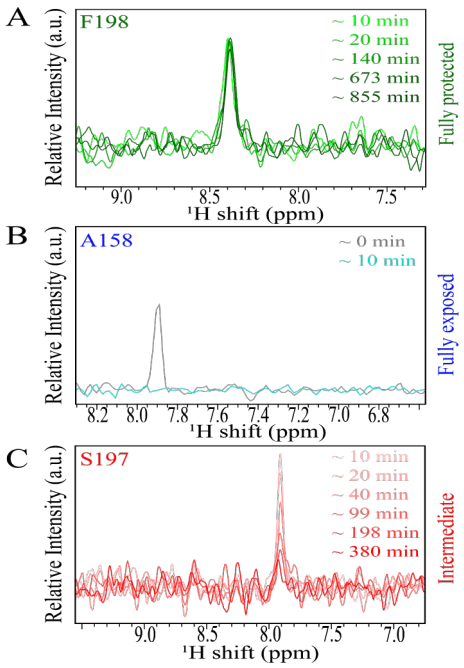

Figure S2: 1D cross-sections from peaks in HSQC spectra acquired during the hydrogen-deuterium exchange (HDX) experiments for the wt and the A211 mutants of PKA R1α (119-379). The panels illustrate representative cases of residues that are fully protected (A) (*e.g.* F198 in wt), fully exposed (B) (*e.g.* A158 in A211D) or subject to intermediate exchange (C) *(e.g.* S197 of A211T). Fully protected residues are defined as those that do not appreciably exchange during the course of the H/D experiments (~14 hours). Fully exposed residues are defined as those for which H/D exchange is complete within the second HSQC acquisition after the dead time of the experiment. Intermediate exchange applies to the residues falling between the fully exposed and fully protected cases. In (B), the first 1D cross-section (gray) is from a control HSQC acquired using the H_2O buffer. In the other panels, lighter shades correspond to 1D cross-section from HSQC spectra recorded at earlier times, while darker shades represent later time points.

Figure S3

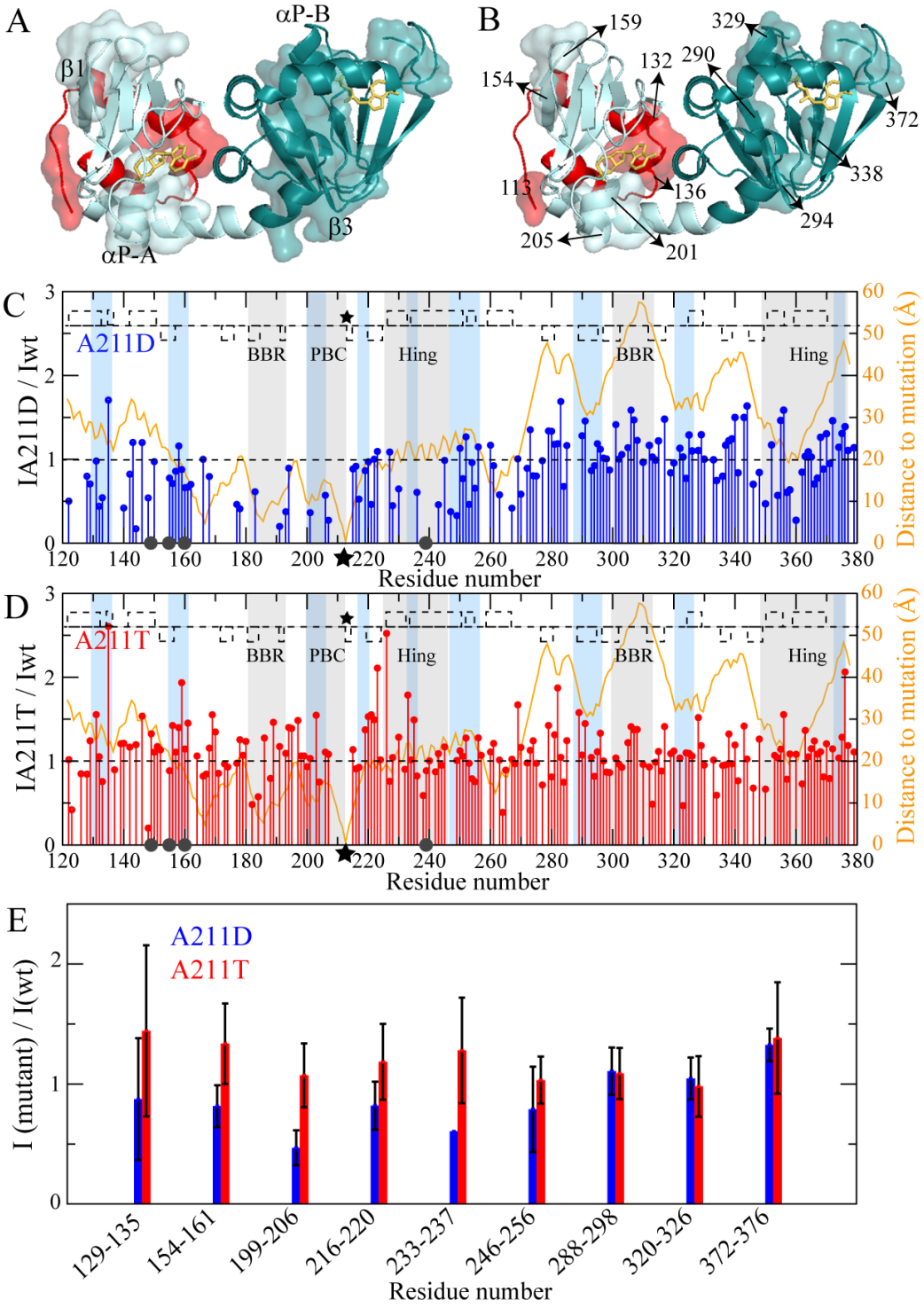

Figure S3: (A) *Aggregation prone sites of wt PKA R1α based on AGGRESCAN* (17) *and* (B) *AmylPred* (18) predictions mapped on the surface of the 1RGS structure, in which N3A-A and the

preceding linker are highlighted in red and the rest of CBD-A is light teal, while CBD-B is in dark teal. cAMP is shown as yellow sticks. Amylpred reports a consensus map among multiple amyloid propensity prediction algorithms, including not only AGGRESCAN but also Amyloidogenic Pattern, Average Packing Density, Beta-strand contiguity, Hexapeptide Conf. Energy, Pafig, SecStr and TANGO. The AmylPred consensus sites are: 34 (not shown), 112-114, 132-137, 154-159, 201-205, 290-294, 325-329, 337-338 and 372-376. Panel A here shows surfaces similar to those shown in Fig. 2 and Fig. S6 albeit with a different color code and it is included here for the convenience of comparison with panel B. (C, D) *Residue-specific intensity changes of A211 mutants relative to wt PKA R1α (119-379) in the presence of 0.7 mM excess cAMP.* Black stars indicate sites of mutation, while the orange line is the distance from the mutated residue. Gray areas highlight allosteric and/or binding hot spots, while the blue areas denote aggregation-prone sites detected by AGGRESCAN. Significantly overlapped residues are removed from these plots. The black circles highlight residues involved in inter-dimer interfaces (Table 1). (E) *Average intensity changes in aggregation prone regions.* The error is the standard deviation of the intensities of all detectable non-overlapped residues in a given region, but for region 233-237 of A211D (marked by *) for which only a single residue was available. The AGGRESCAN aggregation regions were utilized for this panel.

Figure S4

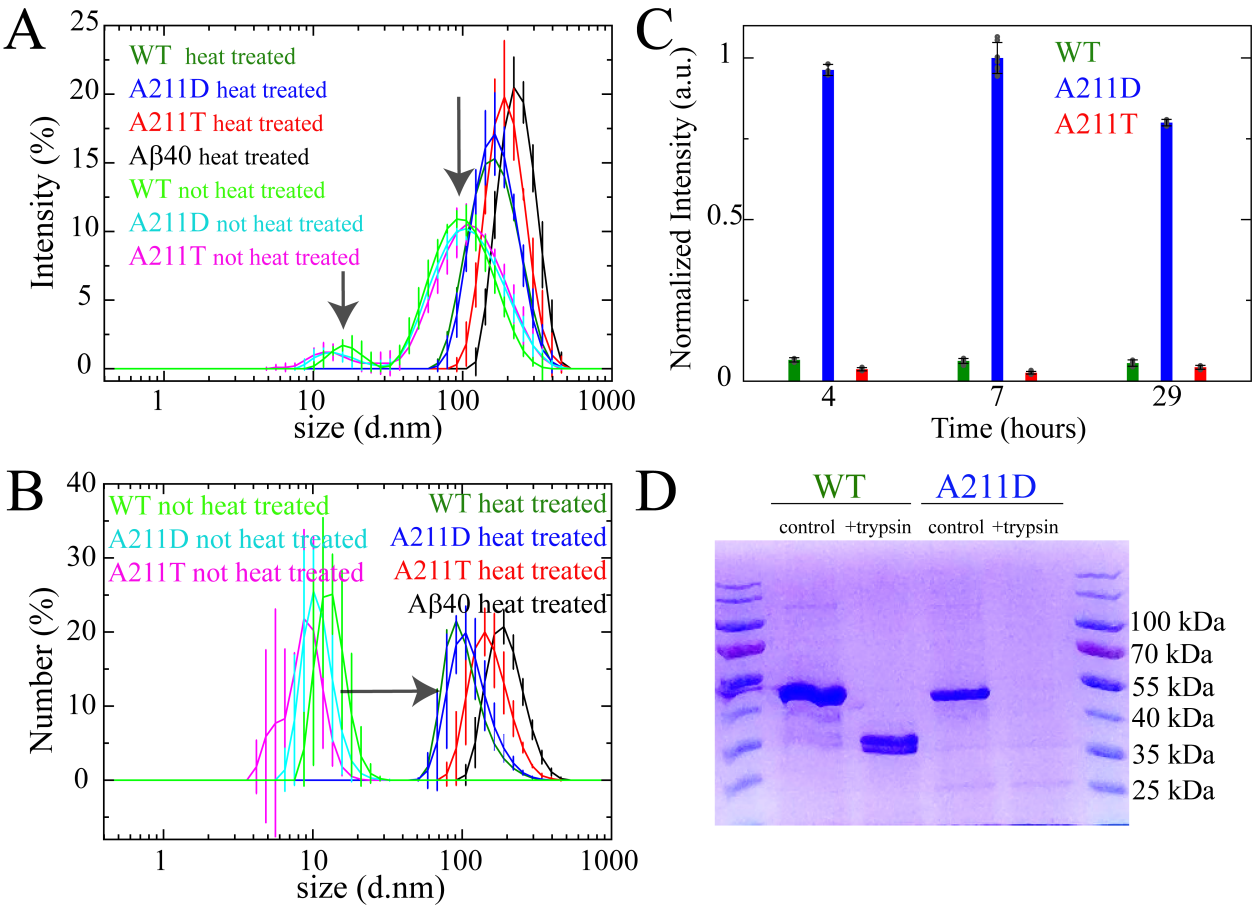

Figure S4: *Dynamic Light Scattering (DLS) Profiles of wt, A211D and A211T PKA R1α Before and After Heat Treatment.* (A) Intensity plot for PKA R1α (8 μM, ten-fold cAMP excess). The negative control samples with no heat treatment exhibit two peaks above 10 nm and at 100 nm. However, after heat-treatment, a single peak is observed corresponding to an average size above 100 nm but slightly below the Aβ(1-40) oligomer size, which serves as a positive control. (B) Relative number plot for PKA R1α (8 μM, ten-fold cAMP excess), showing that most particles in the control samples exhibit a size just above 10 nm. Color codes are shown in the panels. Data acquired in triplicate and error is SD. (C) *PKA R1α Self-Association into Cross β-Sheet Assemblies at 37 °C.* Cross β-sheet formation as reported by ThT binding to 8 μM R1α (1-379) with 10 μM excess cAMP incubated at 37 °C while shaking. The ThT intensity at 482 nm (normalized to the A211D intensity at 7 hours) is higher for the A211D mutant than the wt and A211T mutant. (D) *Differential proteolytic digestion in WT vs. A211D PKA R1α.* Upon an hour incubation at 37 °C, the MW of control samples with no trypsin remains at ~43 kDa, while the samples with trypsin show proteolytic degradation. Proteolysis is more limited in the WT than in the A211D sample.

Figure S5

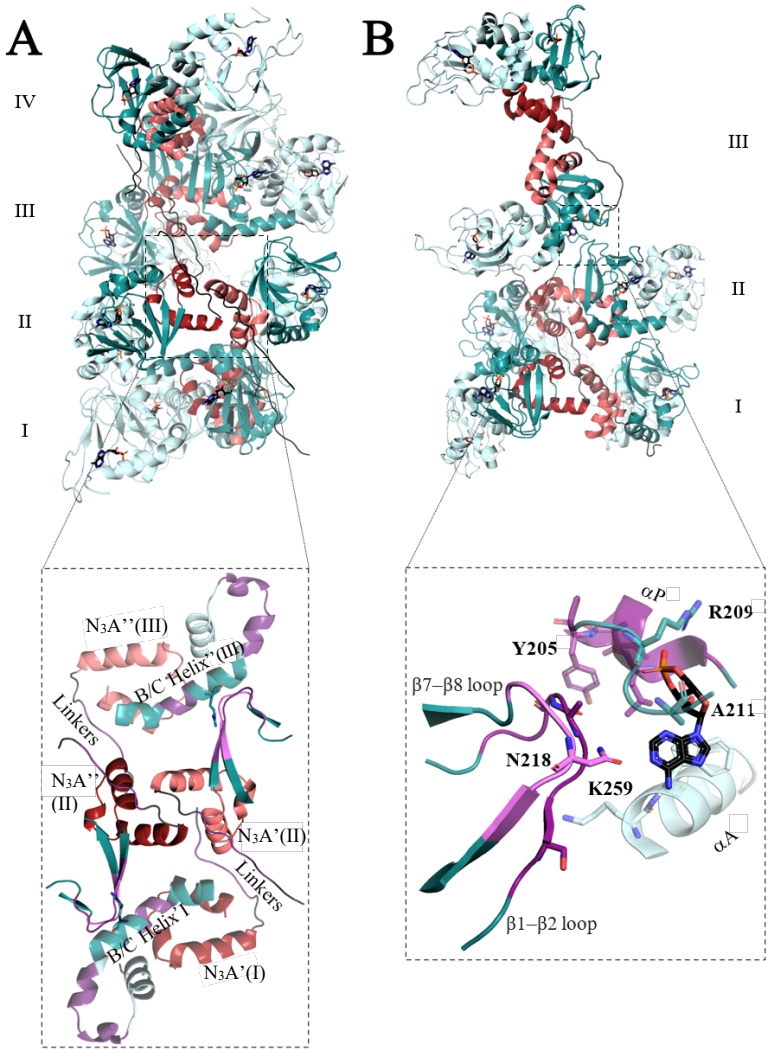

Figure S5: *Comparative Analysis of RIα A211D vs. Wild Type cAMP-Bound Dimers.* The asymmetrical unit of cAMP-bound dimers of A211D RIα (1-379) (A) and wild type RIα (1-379) symmetry mates (PDB code: 4MX3) (B). The unit cell of A211D packs in a R3 space group comprised of four individual dimers (I-IV). In contrast, wild type packs in a $P42_12_12$ space group composed of a single dimer, which we expanded along symmetry mates showing three dimers (I-III). The domains are colored as follows: Linker (Black); N_3A (Red or Salmon); CBD-A (Dark Cyan); CBD-B (Light Cyan). The inset for panel (A) shows details of interface types 2a and 2b in Table 1, including portions of the β1-β2 loops of CBD-A interacting with the B/C Helix (*i.e.* A helix of CBD-B). The inset for panel (B) illustrates details of interface 2c in Table 1, including portions of the β1-β2 loops of CBD-A in one dimer interacting with the αP helix of PBC-A in another dimer. Residues highlighted in shades of purple were identified by AGGRESCAN *in silico*. Interestingly, the A211D mutant dimers packs along several regions identified *in silico* to be prone to aggregation (Figure S3) (19).

Figure S6

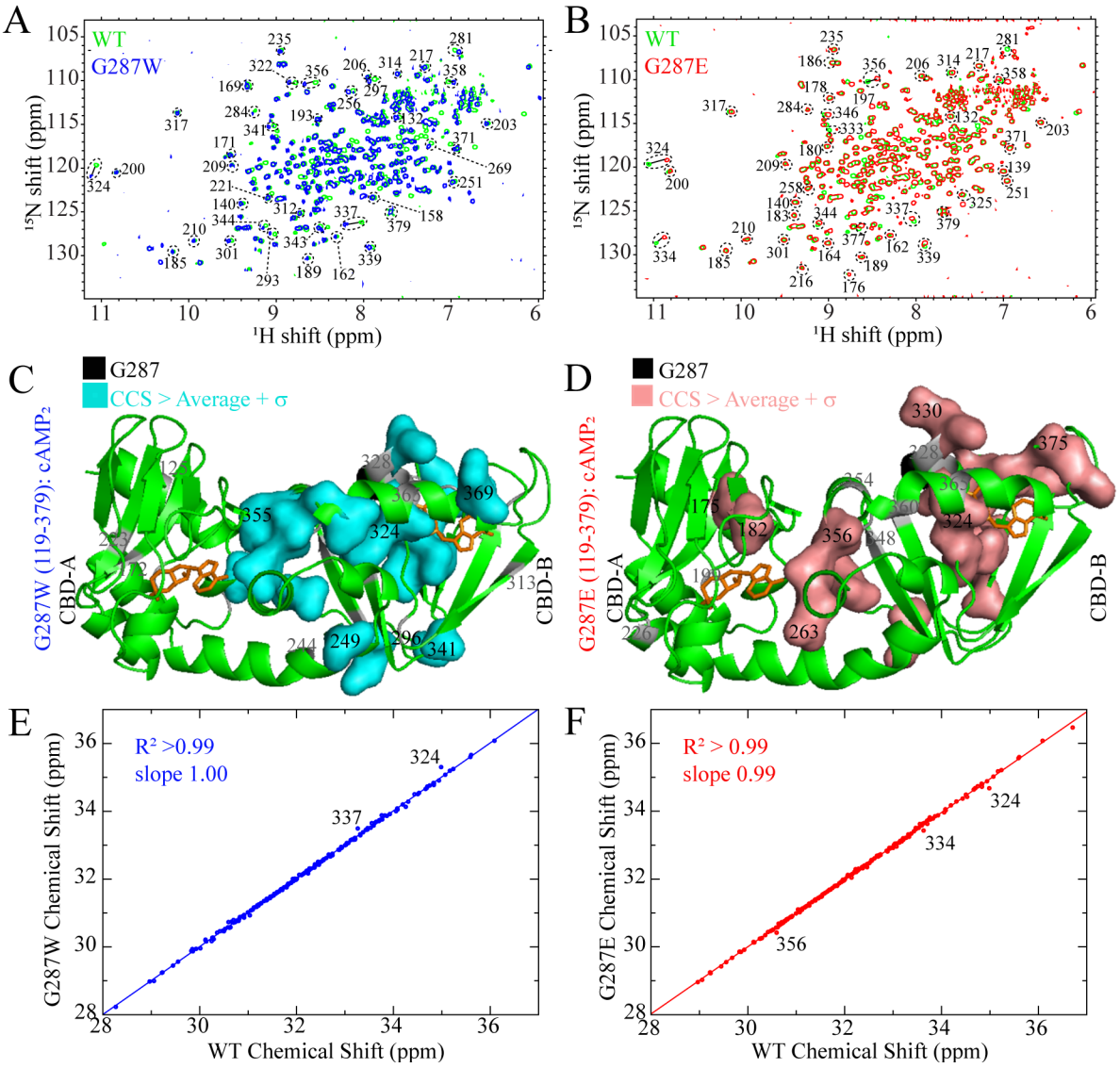

Figure S6: *Chemical Shift Map of the Perturbations Caused by CNC and ACRDYS1 G287 Mutations on the PKA R1α Tandem CBDs.* (A) Overlay of HSQCs spectra of G287W (blue) and wt PKA R1α (119-379) (green) in the presence of 1.2 mM cAMP. (B) As A, but for the G287E mutation. (C) Map of the residues with G287W-induced CCS changes greater than the average plus one standard deviation on the structure of the tandem PKA R1α CBDs bound to cAMP (7). Unassigned or broadened beyond detection residues are highlighted with a gray ribbon. (D) As C, but for the G287E mutation. (E) Correlation between the compounded chemical shifts (CCS) of G287W and wt PKA R1α (119-379) from the spectra in (A). (F) As E, but for the G287E mutation.

Figure S7

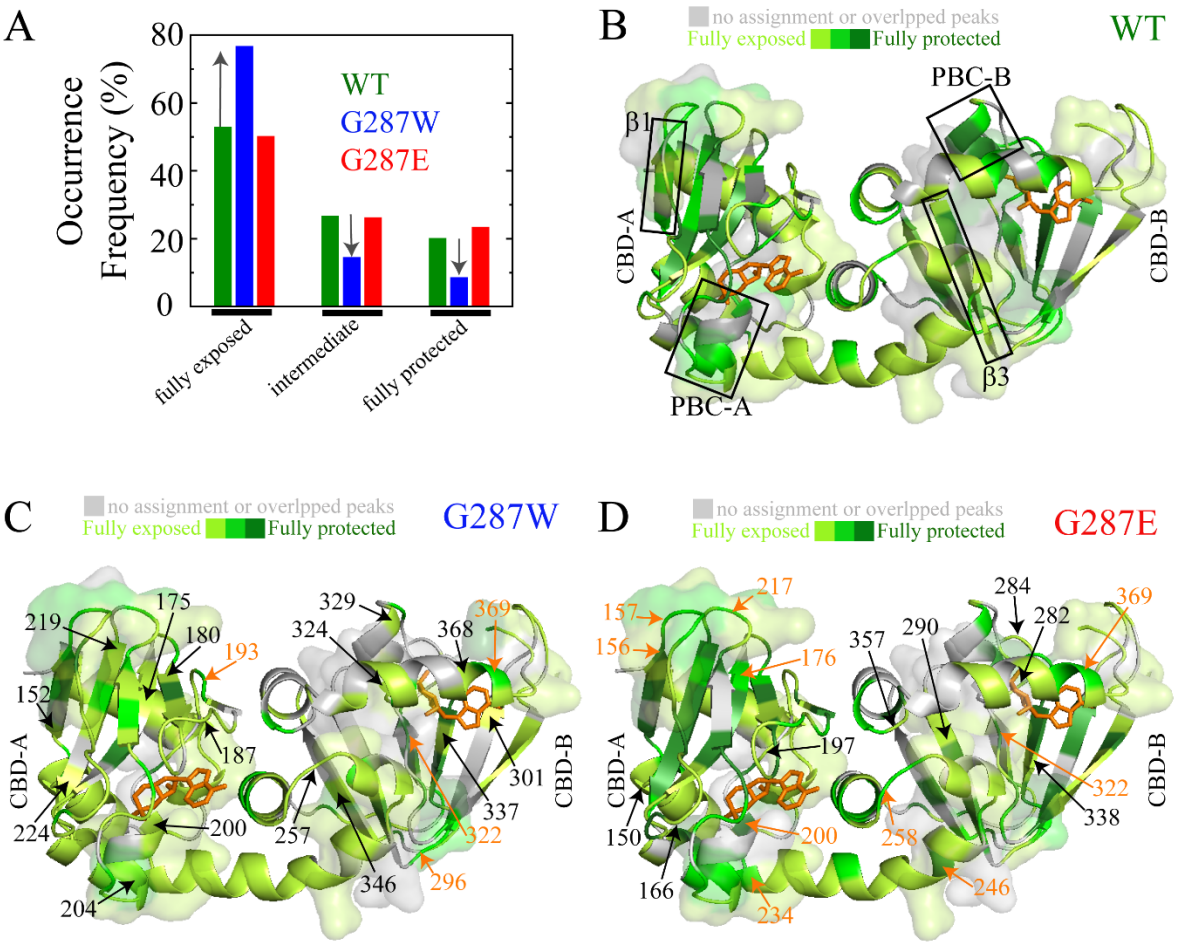

Figure S7: *HDX NMR Map of the Perturbations Caused by CNC and ACRDYS1 G287 Mutations on the PKA R1α Tandem CBDs.* Residue-specific solvent exposure as gauged based on H/D exchange monitored by HSQC spectra for the PKA R1α (119-379) construct in the presence of 0.7 mM excess cAMP. Residues are categorized in three groups as in Figure 2 and S2: fully exposed, intermediate, and fully protected. The cAMP-bound structure (7) is used for all HDX maps. Color codes are shown in the figure. (A) Frequency of occurrence for each exchange class based on the assigned residues. Vertical arrows show the G287W *vs.* wt frequency changes. (B) wt, as in Figure 2C, included here as well for the convenience of comparison. (C) G287W mutant. (D) G287E mutant. Black and orange arrows have the same meaning as in Figure 2. Surfaces in B-D highlight aggregation prone regions as identified by Aggregscan (Fig. S3A).

Figure S8

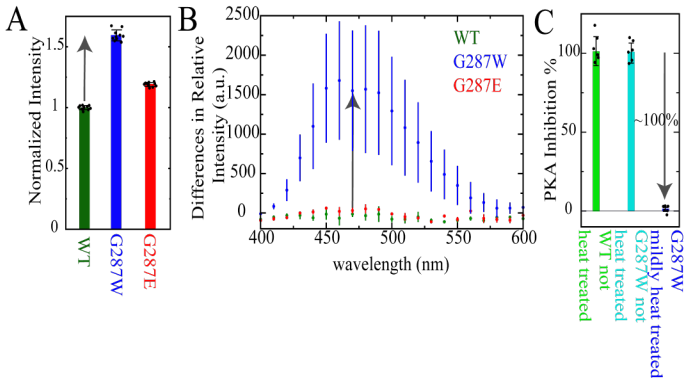

Figure S8: *PKA C Activation by PKA G287W R1α Aggregation.* (A) Normalized ThT fluorescence of 8 μM wt, G287W and G287E PKA R1α measured in the presence of 143 μM cAMP after 13 hours and 20 minutes of incubation at 60 °C. It was ten data points and error is SD. (B) Heat treatment-induced ANS fluorescence intensity difference. Data acquired in duplicate and error is SD. (C) Maximum kinase inhibition by G287W PKA R1α before (cyan) and after (blue) mild heat treatment of 1 μM G287W PKA R1α prior to dilution for the kinase assay. The UV absorbance at 280 nm indicates that the protein is still present in solution even after mild heat treatment, hence the loss of PKA inhibition occurring upon mild heat treatment is not simply the result of precipitation. The wt PKA R1α inhibitory potency (green) is included as a positive control. Six data points and error is SD.

Figure S9

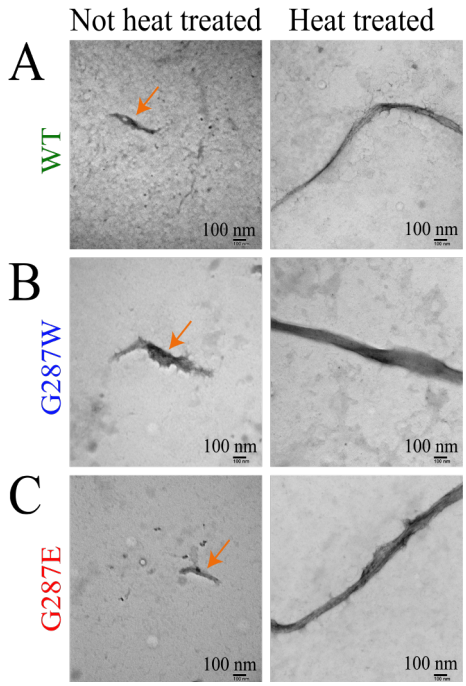

Figure S9: *Morphology of wt, G287W and G287E PKA R1α Assemblies Before and After Heat Treatment.* TEM images of PKA R1α in the presence of ten-fold excess cAMP before and after heat treatment. Horizontal 100 nm bars are indicated in each panel. PKA R1α oligomers with sizes of the order of 100 nm are already present prior to heat treatment (orange arrows), indicating that the heat treatment accelerates oligomerization processes intrinsic to PKA R1α. These observations apply to wt PKA R1α as well as the two G287 mutants. The wt PKA R1α sample used here is distinct from that in Figure S6, showing that aggregate formation is indeed reproducible.

Table S1. *Estimation of A211 Mutants vs. WT PKA R1α Stability (ΔΔG)* [a]

State	PDB Code Construct	Disease	Mutant	ΔΔG (kcal/mol) [b]	RMSD (Å) [c]
cAMP bound	1RGS [d] 91-379 (7)	CNC	A211D	2.04 [g]	0.515
		ACRDYS1	A211T	-10.50	0.661
	3PNA [d] 91-244 (20)	CNC	A211D	3.77	0.232
		ACRDYS1	A211T	0.60	0.230
C-sub bound	6NO7 [e, f] 1-379 (21)	CNC	A211D	1.12	1.310
		ACRDYS1	A211T	-2.77	1.189
	2QCS [f] 91-379 (22)	CNC	A211D	> 10	0.357
		ACRDYS1	A211T	5.33	0.507

[a] Based on the ERIS software implemented with flexible backbone and pre-relaxation.(23) [b] Positive (negative) ΔΔG (kcal/ mol) values indicate that the mutant destabilizes (stabilizes) the structure. [c] The RMSD of the predicted structure compared to the initial WT structure. [d] The cAMP ligands were removed from the PDB file before submission to ERIS. [e] One R1α protomer was removed from the PDB file utilized as ERIS input. [f] The C-subunit was removed from the PDB file used as ERIS input. [g] This value increases to 7.98 kcal/mol for the 1-379 construct in the 4MX3 structure.

Table S2. *Data Collection and Refinement Statistics of the A211D PKA R1α (1-379) Crystal Structure*

	RIα A211D
Data collection	
Space group	R3
Cell dimensions (Å)	
a=b	176.8
c	345.5
No. of dimers per asymmetrical unit	4
Resolution (Å)	4.15
R_{merge}	0.18 (0.46)
Completeness (%)	99.3 (100.0)
I/sigma	12.8 (1.9)
No. reflections	30356
Refinement	
Resolution (Å)	50.0-4.15
R_{work} / R_{free} (%)	22.1/27.0
R.m.s. deviations	
Bond lengths (Å)	0.029
Bond angles (°)	3.2
Ramachandran angles (%)	
most favored	83.4
disallowed	None

Table S3. *A211D vs. WT PKA R1α RMSD Values* [a]

		Single Protomers [b]	**Dimers** [c]
	residues	**<RMSD> ± σ_{RMSD} (Å)**	**<RMSD> ± σ_{RMSD} (Å)**
R1α	109-376	0.8 ± 0.1 [d]	1.6 ± 0.7
CBD-A	109-244	0.6 ± 0.1[d]	1.1 ± 0.3
CBD-B	245-376	1.0 ± 0.1	1.8 ± 1.0

[a] For WT PKA R1a (1-379) the PDB: 4MX3 was used (24). All RMSD values are for backbone atoms. [b] Average over 16 A211D-WT protomer pairs. [c] Average over four A211D dimers. [d] Standard deviation < 0.1.

Table S4. *Estimation of G287 Mutants vs. WT PKA R1α Stability (ΔΔG)* [a]

State	PDB and construct	Disease	Mutant	ΔΔG (kcal/mol) [b]	RMSD (Å) [c]
cAMP bound	4MX3 [d] 1-379 (24)	CNC	G287W	> 10	0.945
		ACRDYS1	G287E	6.98	1.114
	1RGS [d] 91-379 (7)	CNC	G287W	> 10	0.528
		ACRDYS1	G287E	0.81	0.535
C-sub bound	6NO7 [e, f] 1-379 (21)	CNC	G287W	> 10	1.299
		ACRDYS1	G287E	-3.47	1.230
	2QCS [f] 91-379 (22)	CNC	G287W	> 10	0.589
		ACRDYS1	G287E	-3.30	0.725

[a] Based on the ERIS software implemented with flexible backbone and pre-relaxation.(23) [b] Positive (negative) ΔΔG (kcal/ mol) values indicate that the mutant destabilizes (stabilizes) the structure. [c] The RMSD of the predicted structure compared to the initial WT structure. [d] The cAMP ligands were removed from the PDB file before submission to ERIS. [e] One R1α protomer was removed from the PDB file utilized as ERIS input. [f] The C-subunit was removed from the PDB file used as ERIS input.

Supplementary References

1. R. Das, *et al.*, Dynamically driven ligand selectivity in cyclic nucleotide binding domains. *J. Biol. Chem.* **284**, 23682–23696 (2009).
2. E. T. McNicholl, R. Das, S. SilDas, S. S. Taylor, G. Melacini, Communication between tandem cAMP binding domains in the regulatory subunit of protein kinase A-Iα as revealed by domain-silencing mutations. *J. Biol. Chem.* **285**, 15523–15537 (2010).
3. M. Akimoto, *et al.*, Signaling through dynamic linkers as revealed by PKA. *Proc. Natl. Acad. Sci.* **110**, 14231–14236 (2013).
4. K. J. Moleschi, M. Akimoto, G. Melacini, Measurement of state-specific association constants in allosteric sensors through molecular stapling and NMR. *J. Am. Chem. Soc.* **137**, 10777–10785 (2015).
5. M. Akimoto, *et al.*, Mapping the free energy landscape of PKA inhibition and activation: A double-conformational selection model for the tandem cAMP-binding domains of PKA RIα. *PLoS Biol.* **13**, e1002305 (2015).
6. Z. Otwinowski, W. Minor, Processing of X-ray diffraction data collected in oscillation mode. *Methods Enzymol.* **276**, 307–26 (1997).
7. Y. Su, *et al.*, Regulatory subunit of protein kinase A: structure of deletion mutant with cAMP binding domains. *Science (80-.).* **269**, 807–813 (1995).
8. L. C. Storoni, A. J. McCoy, R. J. Read, Likelihood-enhanced fast rotation functions. *Acta Crystallogr. Sect. D Biol. Crystallogr.* **60**, 432–438 (2004).
9. K. Cowtan, Recent developments in classical density modification. *Acta Crystallogr. Sect. D Biol. Crystallogr.* **66**, 470–478 (2010).
10. G. F. Schröder, M. Levitt, A. T. Brunger, Super-resolution biomolecular crystallography with low-resolution data. *Nature* **464**, 1218–1222 (2010).
11. P. Emsley, K. Cowtan, Coot: model-building tools for molecular graphics. *Acta Crystallogr. Sect. D Biol. Crystallogr.* **60**, 2126–2132 (2004).
12. A. T. Brunger, Version 1.2 of the Crystallography and NMR system. *Nat. Protoc.* **2**, 2728 (2007).
13. M. D. Winn, *et al.*, Overview of the CCP 4 suite and current developments. *Acta Crystallogr. Sect. D Biol. Crystallogr.* **67**, 235–242 (2011).
14. M. D. Winn, M. N. Isupov, G. N. Murshudov, Use of TLS parameters to model anisotropic displacements in macromolecular refinement. *Acta Crystallogr. D. Biol. Crystallogr.* **57**, 122–33 (2001).
15. R. A. Laskowski, M. W. MacArthur, D. S. Moss, J. M. Thornton, PROCHECK: a program to check the stereochemical quality of protein structures. *J. Appl. Crystallogr.* **26**, 283–291 (1993).
16. E. Krissinel, K. Henrick, Inference of macromolecular assemblies from crystalline state. *J. Mol. Biol.* **372**, 774–797 (2007).
17. O. Conchillo-Solé, *et al.*, AGGRESCAN: a server for the prediction and evaluation of" hot spots" of aggregation in polypeptides. *BMC Bioinformatics* **8**, 65 (2007).
18. K. K. Frousios, V. A. Iconomidou, C.-M. Karletidi, S. J. Hamodrakas, Amyloidogenic determinants are usually not buried. *BMC Struct. Biol.* **9**, 44 (2009).
19. K. K. Dao, *et al.*, The regulatory subunit of PKA-I remains partially structured and undergoes β-aggregation upon thermal denaturation. *PLoS One* **6**, e17602 (2011).
20. S. Badireddy, *et al.*, Cyclic AMP analog blocks kinase activation by stabilizing inactive

conformation: conformational selection highlights a new concept in allosteric inhibitor design. *Mol. Cell. Proteomics* **10** (2011).
21. T.-W. Lu, *et al.*, Two PKA RIα holoenzyme states define ATP as an isoform-specific orthosteric inhibitor that competes with the allosteric activator, cAMP. *Proc. Natl. Acad. Sci.* **116**, 16347–16356 (2019).
22. C. Kim, C. Y. Cheng, S. A. Saldanha, S. S. Taylor, PKA-I holoenzyme structure reveals a mechanism for cAMP-dependent activation. *Cell* **130**, 1032–1043 (2007).
23. S. Yin, F. Ding, N. V Dokholyan, Eris: an automated estimator of protein stability. *Nat. Methods* **4**, 466–467 (2007).
24. J. G. H. Bruystens, *et al.*, PKA RIα homodimer structure reveals an intermolecular interface with implications for cooperative cAMP binding and Carney complex disease. *Structure* **22**, 59–69 (2014).